

## Fabrication of three dimensional porous silicon distributed Bragg reflectors

D. Mangaiyarkarasi, M. B. H. Breese,<sup>a)</sup> and Y. S. Ow

Department of Physics, Centre for Ion Beam Applications, 2 Science Drive 3,  
National University of Singapore, Singapore 117542, Singapore

(Received 1 September 2008; accepted 7 November 2008; published online 2 December 2008)

Three-dimensional distributed Bragg reflectors, which reflect all incident wavelengths, have been fabricated with micrometer dimensions in porous silicon, resulting in white reflective surfaces when viewed over a wide angular range. Large area arrays of several mm<sup>2</sup> containing many individual micrometer-size pixellated reflectors that can be tuned to reflect a narrow or wide range of wavelengths are designed to appear either as constant or changing reflective images to the naked eye. This work opens avenues in controlling the reflection of light in all directions for applications in wide-angle displays, broadband reflective surfaces for resonant white light emission from semiconductor nanocrystals, and three-dimensional microcavities. © 2008 American Institute of Physics. [DOI: 10.1063/1.3040304]

One-dimensional planar photonic structures based on alternating high and low refractive index porous silicon (PSi) layers are widely used as dielectric mirrors in distributed Bragg reflectors (DBRs) and for resonant emission from microcavities in communications, omnidirectional and tunable mirrors,<sup>1-5</sup> coupled microcavities,<sup>6</sup> modulated light emission,<sup>7</sup> and optical interconnects in future microelectronics.<sup>8,9</sup> They are produced by raising and lowering the hole current density flowing through highly doped *p*-type silicon during anodization, resulting in variations in refractive index.<sup>10,11</sup> We recently demonstrated a highly controlled blueshift<sup>12</sup> of wavelengths reflected from PSi DBRs using ion irradiation where lattice damage increased the wafer resistivity, locally reducing the hole current,<sup>13</sup> resulting in red-green-blue pixels and lines.<sup>14,15</sup> Here individual three-dimensional (3D) DBRs pixels are fabricated with micrometer dimensions, which exhibit different reflective behaviors compared with planar versions, greatly extending the possible applications of this technology. 3D DBR pixels can reflect all incident wavelengths through a wide angular range, resulting in white reflective regions. A combination of different pixel sizes and shapes enables large-area patterned features over many mm<sup>2</sup> that are designed to appear either constant at any illumination angle or changing contrast reflective images by illuminating at different angles.

Figure 1 shows the effect on DBR porous layers across an ion irradiated line for two fluences.<sup>16</sup> Consider the change of the shape of the DBR layers with depth for a fluence of  $2 \times 10^{15}/\text{cm}^2$ . In the first anodization stage [Fig. 1(a)], the layers within the central portion of the irradiated line are thinner than at the unirradiated background. They increase in thickness from the irradiated to the unirradiated side of the boundary, becoming progressively tilted with depth. All anodized layers were then removed and the wafer reanodized under identical conditions to produce a second stage DBR [Fig. 1(b)]. Now the boundary layer tilt angle  $\Psi$  at the surface is that of the final layer of the first stage DBR, and it further increases with depth. First and second stage DBRs thus differ only in their range of  $\Psi$ , which influences the

angular range over which brightest white reflection is subsequently viewed. In practice, brighter reflections are observed from second rather than first stage DBRs where the maximum reflectivity occurs close to near-normal illumination. This process was repeated to give a third stage DBR [Fig. 1(c)]. Here  $\Psi$  has reached a constant value, as indicated by the DBR boundary at the surface being parallel to the underlying Si surface.

Figure 2(a) shows  $\Psi$  versus anodization depth for DBR pixels irradiated with different fluences. For all fluences  $\Psi$  increases approximately linearly with depth until it reaches a constant value due to decoupling between the lower/higher hole current through the irradiated/unirradiated regions as the underlying surface-relief profile evolves.<sup>11</sup> Other fluences produce similar behavior with differing depths over which each stage occurs.  $\Psi$  increases with fluence because the irradiated DBR layers are thinner, resulting in a greater change in layer thickness across the boundary. Inset of Fig. 2(a) indicates that the initial gradient of  $\Psi$  changes linearly with fluence, so adjacent DBR pixels can be produced with dif-

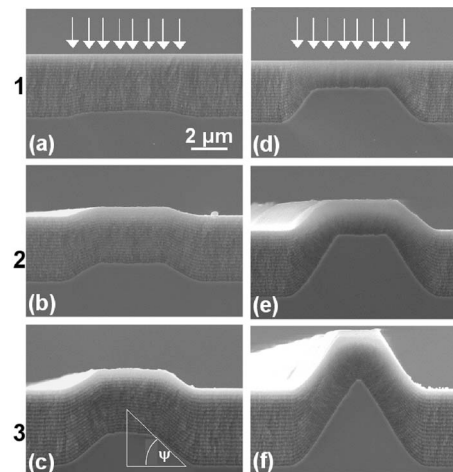


FIG. 1. Cross-sectional SEMs of DBRs formed by irradiating 6  $\mu\text{m}$  wide lines, 2 mm in length with fluences of [(a)–(c)]  $2 \times 10^{15}/\text{cm}^2$  and [(d)–(f)]  $4 \times 10^{15}/\text{cm}^2$ . In (a) and (d), 20 pairs of high/low porosity layers were anodized to a first stage DBR. In (b) and (e), the first stage DBR layers were removed and the same anodization process repeated to give a second stage. In (c) and (f), the same process was repeated to give a third stage DBR.

<sup>a)</sup>Author to whom correspondence should be addressed. Tel.: +65 6516 4953. FAX: +65 6777 6126. Electronic mail: phymbhb@nus.edu.sg.

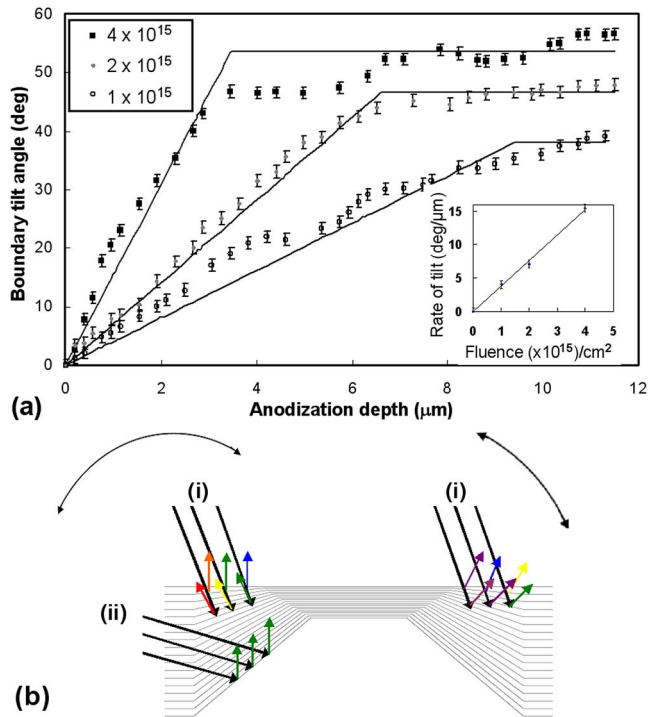


FIG. 2. (Color online) (a) Measured  $\psi$  from Fig. 1 vs anodization depth of the unirradiated background for fluences of  $1 \times 10^{15}/\text{cm}^2$ ,  $2 \times 10^{15}/\text{cm}^2$ , and  $4 \times 10^{15}/\text{cm}^2$ . Inset shows the initial gradient of  $\psi$  vs fluence. (b) Schematic of white light illumination inclined at (i) steep and (ii) shallow angles interacting with a deeply anodized DBR boundary with all layers present.

fering boundary layer tilts simply by varying the fluence. Thus to produce DBR pixels with boundaries which encompass a large range of tilts, layers created close to the original wafer surface are preserved. To produce DBR pixels with parallel boundary layers, a thick layer is first anodized and removed, and then a final DBR formed. Figure 1(f) shows another important feature of prolonged anodization where the flat, central DBR region has disappeared due to the two tilted boundaries meeting. Whereas a DBR with a flat central region reflects normal incidence light normal to the surface, one with only tilted boundaries does not.

Figure 2(b) shows a model of how white light is reflected from a 3D DBR pixel comprising boundary layers where  $\Psi$  changes close to the surface and deeper layers which are parallel. Consider (i) reflections from the left-side boundary of steep illumination using the Bragg equation  $n\lambda = 2d \sin \theta$ , where  $n$  is the order of reflection,  $\lambda$  is the incident wavelength,  $\theta$  is the illumination angle ( $90^\circ$  for normal incidence), and  $d$  is the optical thickness of each layer. Close to the surface, the reflected wavelength is sensitive to changes in layer thickness,  $\lambda \propto d$ , but less so to changes in layer tilt,  $\lambda \propto \sin \theta$ , which varies slowly. At a given position across the boundary, the layer thickness is constant with depth and coherently reflects a particular wavelength. Since the layer thickness changes with position across the boundary, longer/shorter (red/blue) wavelengths are reflected closer to the unirradiated/irradiated sides, resulting in all incident wavelengths reflected so appearing white. The same process occurs in the more tilted layers beneath, which also reflect a wide range of wavelengths through different angles. The right-side boundary reflects light through a complementary range of angles since the layers are tilted in the opposite sense, the combined effect giving a wide angle of reflected

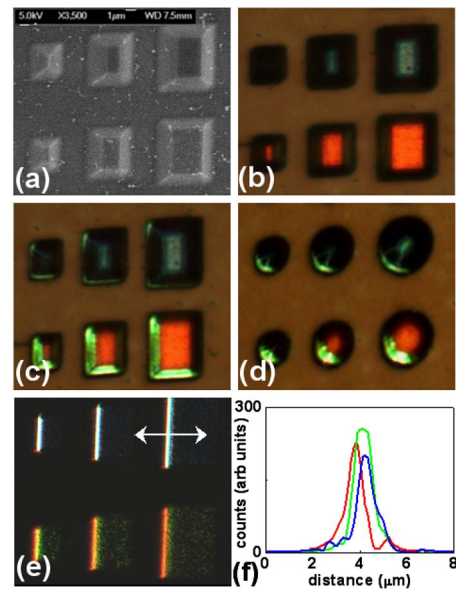


FIG. 3. (Color online) (a) Scanning electron microscope image of deeply anodized (third stage) rectangular DBR pixels. Optical reflection images of this structure under (b) normal and (c) additional inclined illumination from two directions at  $45^\circ$ . (d) Third stage circular pixels under normal and inclined illumination from one direction at  $45^\circ$ . (e) Optical reflection images of shallow anodized (second stage) rectangular DBR pixels under inclined illumination at  $45^\circ$ . (f) Line scan of the recorded red, green, and blue intensities (peaks from left to right) across the region indicated in (e).

light. For (ii) shallow illumination, the more tilted layers deep within the boundary reflect light normal to the surface. These layers are more parallel. So white light will be reflected from the first and second stage DBR boundaries for steep illumination with a more monochromatic reflection for shallow illumination.

Figure 3 demonstrates how white light illumination is reflected normal to the wafer surface from different stages and geometries of individual 3D DBR pixels. Those in the lower and upper rows were irradiated with fluences of  $1 \times 10^{15}/\text{cm}^2$  and  $2 \times 10^{15}/\text{cm}^2$ , respectively, with varying sizes. In Figs. 3(a)–3(d), third stage DBRs were produced. Under normal illumination [Fig. 3(b)], the top, flat DBR pixel surfaces reflect red or blue, depending on the fluence, and the tilted boundaries reflect nothing. With additional inclined illumination [Fig. 3(c)], the boundaries in the lower row reflect green light, i.e., blueshifted compared to the top surface, consistent with Bragg reflection. Hence the reflected light is only observed from the third stage DBR boundaries when the top, flat surface is tuned to reflect long visible wavelengths such as red.

Circular pixels were fabricated under similar conditions and reflect light azimuthally under normal illumination. For inclined illumination [Fig. 3(d)], light is reflected off their curved boundaries in many directions, including normal to the surface. Figure 3(e) shows second stage rectangular DBR pixels fabricated under similar irradiation conditions. For inclined illumination, a wide range of wavelengths is reflected from the DBR boundaries, which appear white across the upper row and as individual colors across the lower row where  $\Psi$  is smaller. Figure 3(f) shows the overlapping red, green, and blue components, with red/blue observed closer to the unirradiated/irradiated boundary sides. Whether the reflected colors overlap or are separately resolved, both appear white to the naked eye.

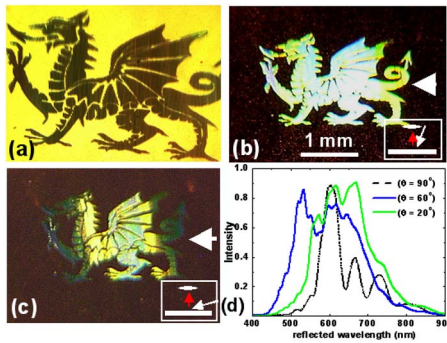


FIG. 4. (Color online) Optical images showing light reflected at normal when illuminated with white light at (a) normal incidence ( $90^\circ$ ), inclined illumination at (b)  $60^\circ$  and (c)  $20^\circ$  to the wafer surface in the horizontal plane. (f) Optical reflectivity spectra recorded from the central portion of the dragon, for different illumination angles.

Consider now many identical or differing pixels producing a reflective pattern of several  $\text{mm}^2$  which is visible to the naked eye. A 3 mm wide Dragon was fabricated as a second stage DBR, comprising 6  $\mu\text{m}$  wide vertical lines, spaced by 6  $\mu\text{m}$ , with the central portion irradiated with a higher fluence. See EPAPS<sup>16</sup> for fabrication and imaging conditions. Under normal illumination, the background of the Dragon appears yellow, owing to light reflected from the gaps between the irradiated lines, with a narrow band of wavelengths observed in Fig. 4(d). The flat, central DBR regions of the irradiated lines reflect little light since irradiation blueshifts the reflected wavelengths beyond the visible range and hence the dragon appears black in Fig. 4(a). Under inclined illumination, the pattern is almost uniformly white [Fig. 4(b)], with wavelengths across the full visible spectrum reflected [Fig. 4(d)]. This demonstrates that white light is reflected from second stage DBRs with different  $\psi$  resulting from different fluence irradiated pixels, still producing uniform white reflection. Under shallow angle illumination individual colors are reflected from different portions [Fig. 4(c)]. Figure 4(d) exhibits a narrower range of wavelengths, consistent with reflection from deeper, more parallel layers.

Another large-area DBR structure was designed to reflect a pattern, which changes with viewing angle. An alphanumeric pattern was produced with each segment irradiated to selectively reflect light only at (i) normal or (ii) over a wide range of viewing angles, or (iii) only over off-normal angles. After producing a second stage DBR, Fig. 5 shows the numerals 9, 5, and 7 reflected with good contrast between those regions which change from “bright” to a “dark” when viewed at progressively shallower angles. Regions which reflect light at (i) normal incidence were uniformly irradiated; (ii) any viewing angle, second stage DBR lines with a flat

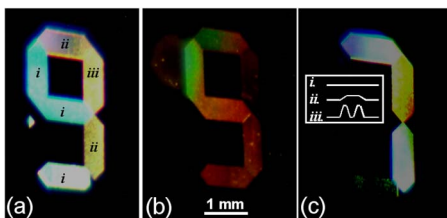


FIG. 5. (Color online) Photographs of reflected light from a patterned alphanumeric display, for progressively shallower white light illumination from (a) to (c). Three different types of patterning and fluences were used in regions (i) to (iii) to create differing reflective behaviors. The cross section of the resultant DBRs produced in each case is shown in (c).

top were produced; and (iii) only under inclined illumination, second stage DBR lines were produced with almost no flat, central region and a steep boundary tilt  $\Psi$ .

In summary, this work demonstrates a combination of high resolution patterning of differing reflectivity across the visible wavelength range. We are able to tailor (i) the range of reflected angles to produce either wide-band (white) reflectivity or single color reflectivity and (ii) the range of angles over which incident light is reflected. While it is possible to achieve wide-band reflectivity on a large-area planar surface with a metallic or a dielectric mirror, and wide-band reflectivity may be achieved over a wide range of incident angles using chirped layers, this has only been reported in the infrared range. This is because chirping relies on a changing layer thickness through many layers, which is not appropriate to the visible range where absorption is more of an issue. Moreover, chirping cannot be used on spatially resolved structures, comprising length scales of micrometers, so it does not provide a means of patterning different reflectivities. Similarly, it is very difficult to vary the peak reflected wavelength on a micrometer lateral scale in metallic mirrors.

This work shows how Bragg reflection through a range of angles for a single beam incident angle is achieved using 3D, tunable PSi DBRs and patterned over wide areas with micrometer resolution. Though this work only describes applications in reflective displays, it opens up other potential uses in controlling the angle and wavelength of emitted light for producing white reflective surfaces for resonant white light emission from semiconductor nanocrystals, 3D individual and coupled optical microcavities, silicon-based lasers, and tunable silicon-based photonic band gap structures for optical modulation.

Funding support by the Singapore Ministry of Education Academic Research Fund Tier 2 under Grant No. T207B1110 is acknowledged.

<sup>1</sup>G. Vincent, *Appl. Phys. Lett.* **64**, 2367 (1994).

<sup>2</sup>L. Pavesi, C. Mazzoleni, A. Tredicucci, and V. Pellegirini, *Appl. Phys. Lett.* **67**, 3280 (1995).

<sup>3</sup>M. Araki, H. Koyama, and N. Koshida, *Appl. Phys. Lett.* **69**, 2956 (1996).

<sup>4</sup>A. Bruyant, G. Lerondel, P. J. Reece, and M. Gal, *Appl. Phys. Lett.* **82**, 3227 (2003).

<sup>5</sup>H. Park, J. H. Dickerson, and S. M. Weiss, *Appl. Phys. Lett.* **92**, 011113 (2008).

<sup>6</sup>M. Ghulinyan, C. J. Oton, G. Bonetti, Z. Gaburro, and L. Pavesi, *J. Appl. Phys.* **93**, 9724 (2003).

<sup>7</sup>S. M. Weiss, H. Ouyang, J. Zhang, and P. M. Fauchet, *Opt. Express* **13**, 1090 (2005).

<sup>8</sup>A. Birner, R. B. Wehrspohn, U. Gösele, and K. Busch, *Adv. Mater. (Weinheim, Ger.)* **13**, 377 (2001).

<sup>9</sup>N. Savage, *IEEE Spectrum* **39**, 32 (2002).

<sup>10</sup>L. Pavesi, *Riv. Nuovo Cimento* **20**, 1 (1997).

<sup>11</sup>V. Lehmann, *Electrochemistry of Silicon* (Wiley-VCH, Weinheim, Germany, 2002).

<sup>12</sup>D. Mangaiyarkarasi, M. B. H. Breese, Y. S. Ow, and C. Vijila, *Appl. Phys. Lett.* **89**, 021910 (2006).

<sup>13</sup>M. B. H. Breese, F. J. T. Champeaux, E. J. Teo, A. A. Bettiol, and D. Blackwood, *Phys. Rev. B* **73**, 035428 (2006).

<sup>14</sup>M. B. H. Breese and D. Mangaiyarkarasi, *Opt. Express* **15**, 5537 (2007).

<sup>15</sup>D. Mangaiyarkarasi, Y. S. Ow, M. B. H. Breese, V. L. Fuh, and E. T. Xiaosong, *Opt. Express* **16**, 12757 (2008).

<sup>16</sup>See EPAPS Document No. E-APPLAB-93-003849 for more details on the (1) fabrication and (2) imaging conditions for the three dimensional pixels. For more information on EPAPS, see <http://www.aip.org/pubservs/epaps.html>.